Pinheiro et al. *EPJ Techniques and Instrumentation* (2023) 10:5
https://doi.org/10.1140/epjti/s40485-023-00093-6

EPJ.org

EPJ Techniques and Instrumentation

RESEARCH ARTICLE

Open Access

Metallacarboranes for proton therapy using research accelerators: a pilot study

Teresa Pinheiro[1,2*], Luís C. Alves[1,3], Victoria Corregidor[1,3], Francesc Teixidor[4], Clara Viñas[4] and Fernanda Marques[1,3]

*Correspondence:
teresa.pinheiro@tecnico.ulisboa.pt
[1]Departamento de Engenharia e Ciências Nucleares, Instituto Superior Técnico, Universidade de Lisboa, Lisboa, Portugal, Estrada Nacional 10, 2695-066, Bobadela LRS, Portugal
[2]IBB, Instituto de Bioengenharia e Biociências, Instituto Superior Técnico, Universidade de Lisboa, Lisboa, Portugal
Full list of author information is available at the end of the article

Abstract

The feasibility of using an external beam microprobe facility to explore the biological effects generated by proton irradiation in cultured cells is demonstrated. An in-air irradiation set-up was developed that allows energy tuning and enables estimating the flux and dose deposition in cells. A pilot study on the effect of boron-rich metallacarboranes as radiosensitizers towards human glioblastoma cells was carried out. This served as a proof of concept for the enhancement effect of proton irradiation induced by the presence of boron, which undergoes a nuclear ^{11}B(p,α)$\alpha\alpha$ reaction. Details of the experimental set-up and physical parameters measured are presented. Also, preliminary results of cell's irradiation and uncertainties are discussed anticipating the advances that have been achieved by our group in this field.

1 Introduction

The use of energetic proton beams offers advantages in cancer treatment including tumour confinement and higher LET (linear energy transfer) than photons. Recently, new prospective drugs with greater selectivity for tumour cells that enable increasing the RBE (relative biological effectiveness) for protons have been investigated. These compounds are constituted by carborane boron clusters, containing 10 atoms of boron each, coordinated by a central metal ion [1]. The theoretical background of the use of metallacarboranes as radiosensitizers is the presence of boron, which may increase the effect of protons on cell death due to the ^{11}B(p,α)$\alpha\alpha$ nuclear reaction [2]. This reaction shows a major resonance near E_p = 0.675 MeV with isotropic distribution and a high cross section of the order of 1 barn. The reaction consists of a two-step sequential decay yielding three α-particles. The de-excitation of ^{12}C, the first intermediate reaction product, yields one α-particle with energy near 4 MeV and ^{8}Be, which in turns splits in two α-particles of 2.74 MeV each [3–5].

Due to these characteristics, the reaction has become very attractive in the context of medical applications of proton therapy as the emitted α-particles range in water is of the order of a cell dimension. In this context, energetic proton beams generated by research accelerators can be useful to demonstrate the potential of metallacarboranes as radiosensitizers for proton therapy. This is very important for proton therapy modality, as there is

Springer

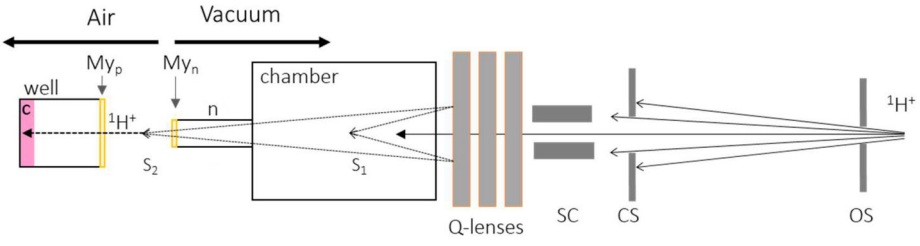

Figure 1 The IST nuclear microprobe schematic (not on scale) including the external beam setup used for cell irradiation. Object slits (*OS*); collimation slits (*CS*); magnetic quadrupole triplet (*Q-lenses*); focus plane inside the irradiation chamber (vacuum) and in-air (S_1) and (S_2), respectively; scanning coils (*SC*); exit nozzle (*n*) supporting a vacuum tight extraction window (My_n). The schematic of the setup for cell irradiation in air represents one unit well of a typical 96-well plate for cell culture. In the used experimental configuration, the extracted $^1H^+$ beam encountered the cell monolayer (*c*) after traversing the air path and a Mylar foil (My_p) which covers the cell culture plate

an urgent need to improve the efficacy of protons in cancer treatment. Thus, enhancing local dose inside tumours upon exposure to radiation, increasing RBE for protons, and reducing the effective radiation dose are factors that ultimately converge to improve the efficacy of treatment [1, 6]. This can be achieved through a synergistic cell-killing effect of metallacarboranes when combined with radiation.

2 Study design

By using research accelerators to generate energetic protons and by extracting the proton beam to air, live cells can be irradiated under controlled conditions, and their dose-dependent viability subsequently assessed. Therefore, a pilot study was planned to demonstrate the enhancement effect of proton-boron reaction in cell-killing. To assess the biological effects, a tumour cell model (human glioblastoma, U87 cells) exposed to metallacarborane compounds (Fe-carborane, FeC, and its iodinated analogue, I_2FeC) was used. The cellular viability as a function of deposited dose will be used as the endpoint for the effect of proton irradiation. Details of the experimental setup, geometry of irradiation, energy tuning of the proton beam, physical parameters measured and calculated as well as cell irradiation protocol will be comprehensively described in the sections below.

3 Experimental setup

Experiments were done at ambient pressure using the external beam facility of the nuclear microprobe (Oxford Microbeams Ltd., UK) installed at the 2.5 MV single ended Van de Graaff accelerator of the IST (Instituto Superior Técnico, Universidade de Lisboa, Portugal) [7, 8]. The technical details of the nuclear microprobe and external beam facility were previously described [8–10].

In Fig. 1 the schematic of the nuclear microprobe and experimental setup used in this study has been depicted. The microprobe configuration consists of object slits for beam size control, collimation slits for beam divergence control, the magnetic quadrupole triplet [7] for beam focusing at the focus plane inside the irradiation chamber (vacuum) and in-air. The scanning coils are located before the lenses.

The beam is extracted from the vacuum chamber to air through an exit nozzle. In the particular set-up used in this study, a nozzle with 2.9 mm internal diameter was used to extract the beam through a 6.3 μm thick Mylar window and scanned over an area of

Table 1 SRIM simulations [11] of transmitted beam energy in the cell layer for an entrance energy of 1.27 MeV protons (simulation n° of particles = 1000; values are x ± SD) and the corresponding value of LET

Cell Layer thickness (μm)	Transmitted beam energy (keV)	LET (keV/μm)
30	477 ± 28	26.43
40	15 ± 21	31.38

interest. The 96-well plate (where the cells are adhered) was positioned perpendicular to the beam path on a x-y-z table. The distance of the sample (cell monolayer at the bottom of the wells) from the exit window was of 13.4 mm. In this pathway besides the 6.3 μm thick Mylar window of the exit nozzle, a 12.6 μm thick Mylar window covering the 96-well plate was used, separating the air path, which is fractionated in two sections, i.e., 2 mm from the exit nozzle to the Mylar cover of the plate and 11.4 mm to the bottom of the well.

The external set-up enables detectors for sample characterization (e.g., PIXE) and accommodates a minicamera that helps on sample visualization and alignment [9, 10].

3.1 Calculation of the energy loss

The proton energy was tuned to ensure that the resonance energy near E_p = 0.675 MeV of the ^{11}B(p,α)$\alpha\alpha$ nuclear reaction was reached at the sample cell layer. Both air and Mylar foils served as energy attenuators for the proton beam. The calculations were carried out using SRIM freeware software [11]. The sequence of attenuators consisted of: (1) Mylar foil of 6.3 μm thickness for extraction of the proton beam from vacuum to air; (2) 2 mm air path; (3) Mylar foil of 12.6 μm thickness covering the 96-well plate where cells were incubated; (4) 11.4 mm air path. Thee proton energy used in this experiment was 1.975 MeV. The proton beam reached the cell layer with an energy of 1.27 MeV. For energy loss calculations the atomic stoichiometry composition and density of Mylar and air was taken from SRIM (Mylar: H8 C10O4, ρ = 0.397; dry air: C1.24 O23.17 N75.52 Ar1.28, ρ = 0.0012 g/cm^3). The energy loss in the cell layer was also simulated with SRIM, considering liquid water as a medium equivalent to a cell. The transmitted beam energy (energy of the proton beam after traversing the cell layer, which corresponds to the proton beam energy at the entrance of the cell layer minus the energy loss thru the cell layer) in 30 μm and 40 μm water (estimated cell layer thickness; see Sect. 4) and corresponding LET is displayed in Table 1.

3.2 Beam focusing and scan size estimation

A proton beam of ∼2.0 MeV was focused using a triplet of quadrupole lenses, Oxford Microbeams Ltd. [7] in air at a distance of 4 mm from the exit nozzle. For routine conditions (with beam currents of ∼100 pA) typical spatial resolution of ∼70 × 70 μm^2 can be achieved [8, 10]. The beam resolution quality can be verified scanning a microscopy copper grid positioned at the chosen focal plane and collecting the induced X-rays with a PIXE detector for obtaining a grid image. (Fig. 2(A)). Most importantly, the grid imaging is an adequate methodology to define the beam scan limits then ensuring that the beam current that can be measured at the in-vacuum chamber is the same as the beam current crossing the nozzle exit foil. The procedure also guarantees that the irradiated area is the same for all the samples analysed in the same run. Routinely, a raster scanning (square of 256 × 256 pixels) is performed by randomly moving the beam over the sample for the defined dimensions. For the positions of the scan not in the circumscribed circle defined

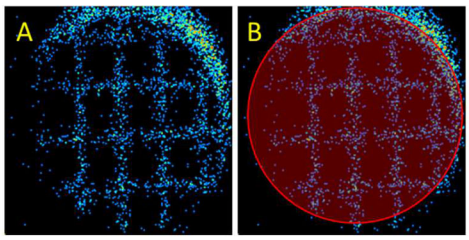

Figure 2 Image of 50-mesh microscopy copper grid obtained by PIXE (*A*) recorded in air at the external microprobe setup and the same image with a mask over-imposed (red circle) delimiting the defined irradiation area (*B*). Grid specifications: 3.05 mm external diameter; pitch 500 μ m; hole 450 μm; bar 50 μm)

Figure 3 Photograph of the Agar P47 phosphor powder pellet (target) during proton irradiation showing the bright fluorescence spot that corresponds to the scanned area (red arrow indicates the diameter of the scan). n—tip of the nozzle (beam extraction system); c—mini-camera

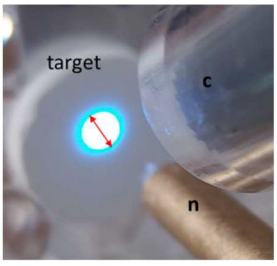

by the exit nozzle, the beam is lost. Therefore, to keep the beam current unchanged in vacuum and in-air, a scan area should be defined to ensure that all the beam can pass the exit nozzle without being trimmed. This can be done by selecting manually a convenient scan geometry and dimension, using the OMDAQ2007 acquisition software features, as shown in Fig. 2(B). The delimited scan area corresponded to a circle including the whole grid image, meaning that for this scan area and dimension the beam is not cropped.

Although the diameter of the exit nozzle (2.9 mm) sets the limit of the maximum scanning area at the exit, beam divergence and lateral straggling across the air path cannot be disregarded. Thus, to obtain more reliable dimensions of the scan at the position of irradiation on the x-y-z table, a commercial material was used (Agar P47 phosphor powder), that emits a bright fluorescence (visible wavelengths) during proton irradiation (Fig. 3). The average size of the irradiated area over 3 runs was 0.134 ± 0.006 cm^2, which represents an uncertainty <5%. The illuminated area of the target provided the best possible estimation of the irradiation area which is required for further calculation of proton flux and dose.

In the context of cell irradiation, other relevant parameter to consider is the homogeneous distribution of particles impinging over the sample surface in the defined circular area. As far as beam stability can be monitored (see Sect. 3.3) the even distribution of protons during irradiation is guaranteed by setting the speed of the scanning (time spent by the beam at each beam position or pixel) at a convenient level (e.g., 10 μs). Therefore, the time required to perform a 256×256 pixels scan is ~0.65 s.

3.3 Charge measurement to estimate the flux of protons impinging on the cell layer

Once our current meter is not accurate for measuring beam currents below 10 pA, in this preliminary study the flux of protons impinging on the cell monolayer was estimated

using EBS (elastic backscattered spectrometry) spectra from a gold reference material positioned at the center of the in-vacuum chamber. Through the Q factor (Q_f) method [12], spectra corrected live charge (Q_{live}) was obtained and proper proton beam current derived as well as spectrum events count rate. In this way a 200 Hz EBS spectrum events count rate was found to correspond to ∼4 pA beam current.

The flux impinging on the cell monolayer can now be estimated as in Eq. (1), where t is the time and e the unit charge:

$$\text{Flux}\left(n^{o}\ of\ protons.cm^{-2}.s^{-1}\right) = \frac{Q_{\text{live}} \times Q_f}{irradiation\ area \times t \times e}. \tag{1}$$

As reference, a spherical cell of 30 μm diameter irradiated with a flux of 2×10^8 protons.cm^{-2}.s^{-1} receives ca. 1400 protons/s.

To obtain the flux of protons arriving at the cell layers of each irradiated well, an average value of the charge measurements carried out during the entire irradiation run for each assay (before starting the irradiation of the wells, 3-wells intercalary measurements and after irradiation) was considered. Uncertainties in flux calculation were in a range of 20% to 40%, mainly due to fluctuations in beam current (measured through the EBS spectrum count rate fluctuations).

4 Irradiation of cell cultures

Glioblastoma U87 cells were grown in 96-well cell plates in an adequate number to form a monolayer. Two Fe carborane compounds, FeC and its iodinated analogue I_2FeC, were used in this study [1]. Cells were incubated for 24 h with FeC and I_2FeC. Non-treated cells served as controls. The concentrations of the compounds were selected according to the cytotoxic activity study previously performed. The medium concentrations of FeC and I_2FeC used in this pilot study were 50 μM and 10 μM, respectively, which correspond to concentrations below the half maximal inhibitory concentration, IC_{50} value.

After the incubation period the culture medium was replaced with fresh medium before irradiation to ensure that only viable cells remain attached to the bottom of the well and that the FeC and I_2FeC compounds taken up by the cells would be responsible for the observed effects. For each assay two sets of controls (non-treated cells) and cells treated with FeC and I_2FeC compounds were prepared, one was irradiated and another was non-irradiated. Twelve wells (one column of the 96-well plate) were considered in each assay for each condition tested, treated and controls, non-irradiated and irradiated (Fig. 4).

Just before proton irradiation, the excess culture medium was removed, ensuring that just the cell monolayer remains adherent at the bottom of the well with culture medium filling interstitial spaces between cells. The U87 cell's dimensions are in the range of 20–30 μm. This way, a water equivalent depth of approximately 30–40 μm can be assumed for the cell layer and cells remain with minimal life supporting conditions until the end of the experiment.

The U87 cells were irradiated for 10 s at ambient pressure with a 1.27 MeV proton beam at the entrance of the cell layer, as described above, to ensure that boron resonance of 675 keV was reached within the cell layer. The effective dimensions of the scanned area of 0.134 cm^2 over the cell layer was ∼33% of the total area of the well, which is 0.32 cm^2. The estimated average dose delivered in each well for a proton flux of 2×10^8 protons.cm^{-2}.s^{-1} was of ∼0.6 Gy/s, whether considering a 30 or 40 μm cell layer thickness.

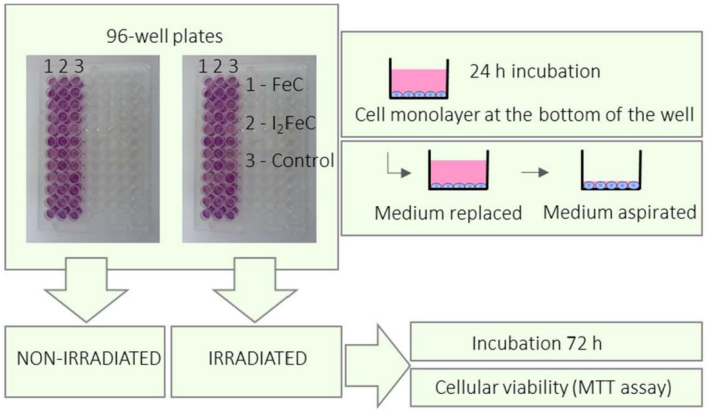

Figure 4 Schematic of the proton irradiation assay

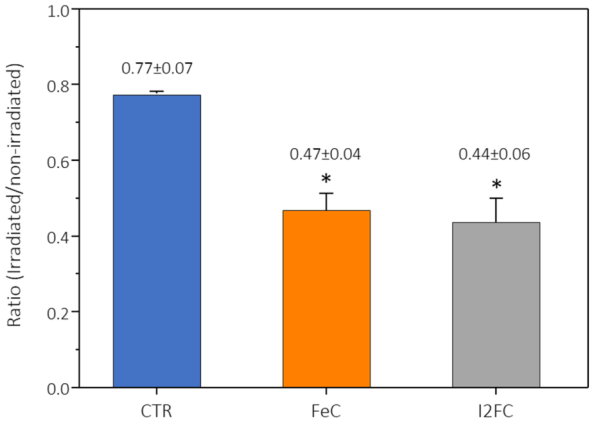

Figure 5 Viability of U87 cells after proton irradiation. Ratios between irradiated and non-irradiated cells for controls and for those cells treated with FeC and I_2FeC compounds are plotted. Significant differences to non-irradiated cells (*) are indicated in the graph ($p < 0.05$)

The cellular viability as a function of deposited dose was used as the endpoint for the effect of proton irradiation. To this end, after U87 cell's irradiation, fresh medium was added, and cellular viability assessed after 72 h incubation using MTT colorimetric assay [13]. In brief the assay measures cell metabolic activity and is based on the enzymatic reduction of tetrazolium dye MTT to a compound which has a purple colour. A decrease of the cellular viability after proton irradiation was observed for U87 cells. In controls, proton irradiation caused a decrease of approximately 20% relative to non-irradiated cells, whereas in FeC and I_2FeC treated cells a significant decrease of ca. 50% was observed (Fig. 5).

Noteworthy, only 33% of the cells in each well were irradiated and the viability assay reflects all the cells in the nonolayer (in each well). Nevertheless, a pronounced decrease in the viability of FeC and I_2FeC treated cells after proton irradiation was observed. The effect cannot be attributed to cytotoxicity of Fe carborane compounds against U87 cells. A screening of cytotoxic activity conducted before irradiation showed that for the concentrations used in this study only a small decrease in viability (5–15%) was observed in

treated cells when compared to controls. All together the results suggest that the significant cell-killing effect is caused by the presence of Fe carborane compounds in cells following proton irradiation. Recent studies reported on the usefulness of other boron cluster's carriers as radiosensitizers for proton therapy using breast cancer [14] and prostate cancer [15] cell lines.

5 Final remarks

The magnitude of the decline in the viability of cells incubated with the boron compounds FeC and its iodinated analogue I_2FeC, was well above the direct effects caused by proton irradiation alone in non-treated cells. These compounds have very interesting biological properties, such as efficient intracellular uptake and low toxicity [16]. The viability decrease observed in our study may derive from synergistic effects of α-particles generated in the proton-boron nuclear reaction. These particles may have direct consequences in the irradiated cells where they are generated and possibly in those contiguous to the irradiated area. The estimated range of these α-particles in water is of the order of 16–25 μm, which is in the range of a U87 cell dimension. The energy of the generated α-particles can induce DNA damage and impairing tumour cells growth. These effects may add to damages caused directly by the proton beam, as the nuclear reaction resonance of 675 keV is in the range of energies of the Bragg peak. In this context energetic proton beams generated by research accelerators would be useful to demonstrate the potential of boron-rich clusters as radiosensitizers. By increasing the delivery of boronated compounds to tumour cells a larger impact of the proton-boron nuclear reaction in cell-killing would be expected as the distribution of energy through the cells will improve. This would contribute to dose enhancement and enable to increase the RBE for protons, making proton therapy more efficient in terms of dose delivery.

A major limitation of this work refers to the uncertainties in charge determination and therefore on the estimation of dose. Improvements in the experimental setup are ongoing to collect charge during irradiation period of each well. In addition, a validation step with a Monte Carlo (MC) model is being performed to compare several MC and experimental parameters, such as divergence of the beam, energy spectrum, the variation of the Bragg peak depending on the point of reaction and the variation of the maximum dose. Therefore, dosimetry MC results will be very useful to the optimization of the experimental cell irradiation setup.

Finally, this pilot study provided evidences for the proof of concept that Fe carboranes, FeC and I_2FeC compounds magnify cell-killing after proton irradiation, acting as radiosensitizers and that the mechanism may be associated with the presence of boron inside the cells and the nuclear reaction with protons.

Acknowledgements
Not applicable.

Funding
The authors received support from: FCT—Fundação para a Ciência e Tecnologia in the scope of the projects UID/Multi/04349/2019, PTDC/MEDQUI/29649/2017 of the Centro de Ciências e Tecnologias Nucleares C^2TN, and UIDP/04565/2020 and LA/P/0140/2020—Associate Laboratory Institute for Health and Bioeconomy i4HB of the Instituto de Bioengenharia e Biociências IBB; Spanish Ministerio de Economía y Competitividad (PID2019-106832RB-I00) and the Generalitat de Catalunya (2017SGR1720).

Availability of data and materials
Not applicable.

Declarations

Competing interests
The authors declare no competing interests.

Author contributions
Conceptualization, FM and TP; methodology, LCA, TP, and VC; metallacarborane compounds synthesis, CV and FT; formal analysis, FM, LCA, and TP; writing—original draft preparation, TP and LCA; writing—review and editing, all the authors. All authors read and approved the final manuscript.

Author details
[1]Departamento de Engenharia e Ciências Nucleares, Instituto Superior Técnico, Universidade de Lisboa, Lisboa, Portugal, Estrada Nacional 10, 2695-066, Bobadela LRS, Portugal. [2]IBB, Instituto de Bioengenharia e Biociências, Instituto Superior Técnico, Universidade de Lisboa, Lisboa, Portugal. [3]Centro de Ciências e Tecnologias Nucleares, Instituto Superior Técnico, Universidade de Lisboa, Lisboa, Portugal. [4]Institut de Ciència de Materials de Barcelona (ICMAB-CSIC), Campus UAB, 08193 Bellaterra, Barcelona, Spain.

Publisher's Note

Received: 31 October 2022 Accepted: 15 February 2023 Published online: 09 March 2023

References

1. García-Mendiola T, Bayon-Pizarro V, Zaulet A, Fuentes I, Pariente F, Teixidor F, Viñas C, Lorenzo E. Metallacarboranes as tunable redox potential electrochemical indicators for screening of gene mutation. Chem Sci. 2016;7:5786–97.
2. Yoon D-K, Jung J-Y, Suha TS. Application of proton boron fusion reaction to radiation therapy: a Monte Carlo simulation study. Appl Phys Lett. 2014;105:223507.
3. Moreau DC. Potentiality of the proton-boron fuel for controlled thermonuclear fusion. Nucl Fusion. 1977;17:13–20.
4. Spraker MC, Ahmed MW, Blackston MA, Brown N, France RH III, Henshaw SS, Perdue BA, Prior RM, Seo P-N, Stave S, Weller HR. The ^{11}B(p,α)^{8}Be $\rightarrow \alpha + \alpha$ and the ^{11}B(α,α)^{11}B reactions at energies below 5.4 MeV. J Fusion Energy. 2012;31:357–67.
5. Ruggiero AG. Nuclear Fusion of Protons with Boron. Contribution to Conference on Prospects for Heavy Ion Inertial Fusion, Aghia Pelaghia, Crete, Greece, September 26–October 1 (1992). https://inis.iaea.org/collection/NCLCollectionStore/_Public/24/028/24028563.pdf (accessed 9-6-2022).
6. Cirrone GAP, Manti L, Margarone D, Petringa G, Giuffrida L, Minopoli A, Picciotto A, Russo G, Cammarata F, Pisciotta P, Perozziello FM, Romano F, Marchese V, Milluzzo G, Scuderi V, Cuttone G, Korn G. First experimental proof of Proton Boron Capture Therapy (PBCT) to enhance protontherapy effectiveness. Sci Rep. 2018;8:1141.
7. http://www.microbeams.co.uk/ (accessed 9-6-2022).
8. Alves LC, Breese MBH, Alves E, Paúl A, da Silva MR, da Silva MF, Soares JC. Micron-scale analysis of SiC/SiCf composites using the new Lisbon nuclear microprobe. Nucl Instrum Methods B. 2000;161–163:334–8.
9. Corregidor V, Alves LC, Barradas NP, Reis MA, Marques MT, Ribeiro JA. Characterization of Mercury gilding art objects by external proton beam. Nucl Instrum Methods B. 2011;269:3049–53.
10. Corregidor V, Oliveira AR, Rodrigues PA, Alves LC. Paintings on copper by the Flemish artist Frans Francken II: PIXE characterization by external beam. Nucl Instrum Methods B. 2015;348:291–5.
11. http://www.srim.org (accessed 9-6-2022).
12. Grime GW. The "Q factor" method: quantitative microPIXE analysis using RBS normalisation. Nucl Instrum Methods B. 1996;109/110:170–4.
13. Marques A, Belchior A, Silva F, Marques F, Campello MPC, Pinheiro T, Santos P, Santos L, Matos APA, Paulo A. Dose rate effects on the selective radiosensitization of prostate cells by GRPR-targeted gold nanoparticles. Int J Mol Sci. 2022;23:5279.
14. Murphy N, McCarthy E, Dwyer R, Farràs P. Boron clusters as breast cancer therapeutics. J Inorg Biochem. 2021;218:111412.
15. Bláha P, Feoli C, Agosteo S, Calvaruso M, Cammarata FP, Catalano R, Ciocca M, Cirrone GAP, Conte V, Cuttone G, Facoetti A, Forte GI, Giuffrida L, Magro G, Margarone D, Minafra L, Petringa G, Pucci G, Ricciardi V, Rosa E, Russo G, Manti L. The proton-boron reaction increases the radiobiological effectiveness of clinical low- and high-energy proton beams: novel experimental evidence and perspectives. Front Oncol. 2021;11:682647.
16. Nuez-Martínez M, Queralt-Martín M, Muñoz-Juan A, Aguilella VM, Laromaine A, Teixidor F, Viñas C, Pinto CG, Pinheiro T, Guerreiro JF, Mendes F, Roma-Rodrigues C, Baptista PV, Fernandes AR, Valic R, Marques F. Boron clusters (ferrabisdicarbollides) shaping the future as radiosensitizers for multimodal (chemo/radio/PBFR) therapy of glioblastoma. J Mater Chem B. 2022;10:9794–815.